Vortices in dipolar Bose–Einstein condensates in synthetic magnetic field*

Qiang Zhao(赵强)[1,2] and Qiang Gu(顾强)[1,†]

[1] *Department of Physics, University of Science and Technology Beijing, Beijing* 100083, *China*
[2] *School of Science, North China University of Science and Technology, Tangshan* 063009, *China*

(Received 20 October 2015; published online 30 November 2015)

We study the formation of vortices in a dipolar Bose–Einstein condensate in a synthetic magnetic field by numerically solving the Gross–Pitaevskii equation. The formation process depends on the dipole strength, the rotating frequency, the potential geometry, and the orientation of the dipoles. We make an extensive comparison with vortices created by a rotating trap, especially focusing on the issues of the critical rotating frequency and the vortex number as a function of the rotating frequency. We observe that a higher rotating frequency is needed to generate a large number of vortices and the anisotropic interaction manifests itself as a perceptible difference in the vortex formation. Furthermore, a large dipole strength or aspect ratio also can increase the number of vortices effectively. In particular, we discuss the validity of the Feynman rule.

Keywords: dipolar condensates, vortex, synthetic magnetic field

PACS: 67.85.De, 03.75.Hh, 05.30.Jp **DOI:** 10.1088/1674-1056/25/1/016702

1. Introduction

Since the recent experimental realization of Bose–Einstein condensations (BECs) of ^{52}Cr,[1] ^{164}Dy,[2] and ^{168}Er,[3] which have magnetic dipole moments of $6\mu_B$, $7\mu_B$, and $10\mu_B$, respectively, much effort has been devoted to understanding the physics of dipolar BECs.[4,5] The two most important characteristics of the dipole–dipole interaction (DDI) are its long range and anisotropic nature, which give rise to a few striking experimental signatures, such as rich spin textures,[6,7] modified low-lying excitations,[8] and strong dipolar nature of a quantum ferrofluid.[9]

One important issue in connection to the BECs is that the vortex formation and structure exhibit various novel physical phenomena under the influence of the dipolar interaction, together with other interactions and geometries. The vortices with different symmetries such as triangular, square, stripe-like, and bubble-like were theoretically explored.[10–12] The ground state of a rotating BECs displays a rich variety of vortex patterns, such as flower-like lattice, crescent, and snake-skin piebald.[13–15] In Ref. [16], the d-wave symmetric collapse and explosion of the condensate were experimentally observed, and the formation of vortex rings with opposite circulations was theoretically predicted.

All the aforementioned studies pertain to systems in which the vortices are created in a rotating frame of reference. It is similar to the rotating-bucket method of conventional low-temperature physics,[17–19] where a vortex is obtained by rotating a bucket full of water. Recently, Lin *et al.*[20,21] performed an experimental study of a synthetic magnetic field. As soon as the synthetic field exceeds a critical one, vortices enter the condensate and the number of vortices increases as the synthetic magnetic field strength increases. The author suggested that this method has advantages in comparison to a rotating frame, the latter is difficult to add optical lattices and large angular momenta, and the rotation is limited by heating and metastability.

Motivated by the pioneering experiment, we are interested in the formation of vortices in a synthetic magnetic field. This issue has been discussed in a BEC with only contact interaction.[22] In this paper, we investigate how the vortices behave under a synthetic magnetic field if DDI is added. For this goal, we consider a two-dimensional (2D) system that is confined in the xy plane with relatively large trap frequency ω_z. We make an extensive comparison of the vortices generated by the two methods. Numerical results indicate that anisotropic superfluidity manifests itself as the directional dependence of the vortex formation. For the rotating frame, a key observation is that the system undergoes a transition from triangular lattice to stripe pattern when the rotating frequency approaches the upper limit. For the synthetic magnetic field case, the vortex row number and the vortex number are much smaller than those calculated for the rotating frame.

This paper is organized as follows. In Section 2, we outline the Gross–Pitaevskii (GP) equation for a dipolar BEC under a synthetic magnetic field in a 2D system. Details about how the numerical method is used are given. In Section 3, we study the properties of the system with various parameters, including the dipole strength, the rotating frequency, the aspect

*Project supported by the National Natural Science Foundation of China (Grant No. 11274039), the National Basic Research Program of China (Grant No. 2013CB922002), and the Fundamental Research Funds for the Central Universities of China.

†Corresponding author. E-mail: qgu@ustb.edu.cn

© 2016 Chinese Physical Society and IOP Publishing Ltd

ratio of the trap, and the orientation of the dipole moment of the atoms. It is shown that the behaviors of the system in the synthetic magnetic field are quite different compared to those in the rotating frame. Section 4 gives a brief conclusion.

2. Formulation

2.1. Gross–Pitaevskii equation

Consider a system of bosonic neutral atoms of mass m. In the weak interaction limit, the dipolar condensate in a synthetic magnetic field can be described by the non-local GP equation

$$\mathrm{i}\hbar\frac{\partial\psi(\boldsymbol{r},t)}{\partial t} = \left[\frac{1}{2m}(\boldsymbol{P}-\boldsymbol{A})^2+V(\boldsymbol{r})+g|\psi|^2 + V_{\mathrm{dip}}(\boldsymbol{r},t)\right]\psi(\boldsymbol{r},t), \quad (1)$$

where $\psi(\boldsymbol{r},t)$ is the macroscopic wave function of the condensate and is normalized to the total number of particles N, and $g=4\pi\hbar^2 a_{\mathrm{s}}/m$ represents the strength of the contact interaction between atoms with s-wave scattering length a_{s}. The harmonic trapping potential $V(\boldsymbol{r})=\frac{1}{2}m(\omega_x^2x^2+\omega_y^2y^2+\omega_z^2z^2)$, where ω_j with $j=x,y,z$ are the trap frequencies along the three coordinate axes. The $\boldsymbol{P}$ is the canonical momentum operator. We assume that uniform magnetic field $\boldsymbol{B}$ is parallel to the z axis. The field is such that half the cyclotron frequency $\omega_{\mathrm{c}}=B/2m$ (in units of charge divided by the light velocity) is identified with the rotating frequency $\boldsymbol{\Omega}$, and the vector potential in the symmetric gauge is $\boldsymbol{A}=(\boldsymbol{B}\times\boldsymbol{r})/2=m(\boldsymbol{\Omega}\times\boldsymbol{r})$.

The mean-field dipolar interaction term $V_{\mathrm{dip}}(\boldsymbol{r},t)$ is given by the convolution

$$V_{\mathrm{dip}}(\boldsymbol{r},t)=\int \mathrm{d}\boldsymbol{r}'v_{\mathrm{dip}}(\boldsymbol{r}-\boldsymbol{r}')|\Psi(\boldsymbol{r}',t)|^2, \quad (2)$$

with DDI

$$v_{\mathrm{dip}}(\boldsymbol{r}-\boldsymbol{r}')=\frac{C_{\mathrm{dd}}}{4\pi}\frac{1-3\cos^2\theta}{|\boldsymbol{r}-\boldsymbol{r}'|^3}, \quad (3)$$

where $|\boldsymbol{r}-\boldsymbol{r}'|$ is the distance between the dipoles. We assume that the atoms have a non-zero dipole moment, and all the dipoles are aligned to an external field, which is in the xz plane and forms an angle θ with the z axis. Thus the dipolar axis $\boldsymbol{n}=(n_1,n_2,n_3)=(\sin\theta,0,\cos\theta)$. The coupling constant $C_{\mathrm{dd}}=d^2/\varepsilon_0$ when the atoms have an electric dipole moment d, where ε_0 is the permittivity of the vacuum. When the atoms have a magnetic dipole moment μ_{d}, $C_{\mathrm{dd}}=\mu_0\mu_{\mathrm{d}}^2$, where μ_0 is the permeability of free space. For the dipolar condensate with contact interaction, one can introduce a natural dimensionless parameter to characterize the relative strength of the dipole and the s-wave interactions, $\varepsilon_{\mathrm{dd}}=C_{\mathrm{dd}}/3g$.

Before proceeding further, we transform the GP equation into a dimensionless form, where the spatial coordinates are normalized by the characteristic harmonic oscillator length $a_0=\sqrt{\hbar/(m\omega)}$ with $\omega=\min\{\omega_x,\omega_y,\omega_z\}$, the time and energy are in units of ω^{-1} and $\hbar\omega$, respectively. Then the dimensionless GP equation is given by[23]

$$\mathrm{i}\frac{\partial\tilde{\psi}(\tilde{\boldsymbol{r}},\tilde{t})}{\partial\tilde{t}} = \left[\frac{1}{2}(\tilde{\boldsymbol{P}}-\tilde{\boldsymbol{A}})^2+V(\tilde{\boldsymbol{r}})+\beta(1-\varepsilon_{\mathrm{dd}})|\tilde{\psi}|^2 + \tilde{\Phi}_{3\mathrm{D}}(\tilde{\boldsymbol{r}},\tilde{t})\right]\tilde{\psi}(\tilde{\boldsymbol{r}},\tilde{t}), \quad (4)$$

$$\tilde{\Phi}_{3\mathrm{D}}(\tilde{\boldsymbol{r}},\tilde{t}) = -3\beta\varepsilon_{\mathrm{dd}}\partial_{\tilde{\boldsymbol{n}}\tilde{\boldsymbol{n}}}\int \mathrm{d}\tilde{\boldsymbol{r}}'U_{3\mathrm{D}}(\tilde{\boldsymbol{r}}-\tilde{\boldsymbol{r}}')|\tilde{\Psi}(\tilde{\boldsymbol{r}}',\tilde{t})|^2, \quad (5)$$

where $\beta=4\pi Na_{\mathrm{s}}/a_0$, the kernel $U_{3\mathrm{D}}(\tilde{\boldsymbol{r}}-\tilde{\boldsymbol{r}}')=1/4\pi|\tilde{\boldsymbol{r}}-\tilde{\boldsymbol{r}}'|$, $\partial_{\tilde{\boldsymbol{n}}}=n_1\partial_{\tilde{x}}+n_2\partial_{\tilde{y}}+n_3\partial_{\tilde{z}}$ is the derivative along the dipole axis, and $\partial_{\tilde{\boldsymbol{n}}\tilde{\boldsymbol{n}}}=\partial_{\tilde{\boldsymbol{n}}}(\partial_{\tilde{\boldsymbol{n}}})$, $V(\tilde{\boldsymbol{r}})=(\gamma_x^2\tilde{x}^2+\gamma_y^2\tilde{y}^2+\gamma_z^2\tilde{z}^2)/2$, and $\gamma_j=\omega_j/\omega$ with $j=x,y,z$, in which γ_z is the aspect ratio of the trapping potential. In order to simplify the notations, we will show the variables without tildes in the rest of the paper except where mentioned otherwise. In the present work, we consider a quasi-2D trap which satisfies $\gamma_z\gg\gamma_x=\gamma_y=1$. In this case, the motion of the atoms is frozen along the z direction. This allows us to use an ansatz for the order parameter in the form $\psi(\boldsymbol{r},t)=\psi_{2\mathrm{D}}(x,y,t)\psi_{1\mathrm{D}}(z)\mathrm{e}^{-\mathrm{i}\gamma_z t/2}$, with $\psi_{1\mathrm{D}}(z)=(\gamma_z/\pi)^{1/4}\mathrm{e}^{-\gamma_z z^2/2}$ denoting the harmonic oscillator ground state along the axial direction. After integrating out the axial coordinate, a 2D dimensionless GP equation can be obtained[23]

$$\mathrm{i}\frac{\partial\psi_{2\mathrm{D}}(x,y,t)}{\partial t} = \left\{\frac{1}{2}(\boldsymbol{P}-\boldsymbol{A})^2+\frac{1}{2}(x^2+y^2)+\Phi_{2\mathrm{D}} +\beta\sqrt{\frac{\gamma_z}{2\pi}}\left[1-\varepsilon_{\mathrm{dd}}\left(1-3n_3^2\right)\right]|\psi_{2\mathrm{D}}|^2\right\}\psi_{2\mathrm{D}}(x,y,t), \quad (6)$$

$$\Phi_{2\mathrm{D}} = -\frac{3\beta\varepsilon_{\mathrm{dd}}}{2}\left[\partial_{\boldsymbol{n}_\perp\boldsymbol{n}_\perp}-n_3^2\nabla^2\right] \times\int \mathrm{d}x'\mathrm{d}y'U_{2\mathrm{D}}(x-x',y-y')|\psi_{2\mathrm{D}}(x',y',t)|^2, \quad (7)$$

where $\nabla^2=\partial^2/\partial x^2+\partial^2/\partial y^2$, $\partial_{\boldsymbol{n}_\perp}=n_1\partial_x+n_2\partial_y$, and $\partial_{\boldsymbol{n}_\perp\boldsymbol{n}_\perp}=\partial_{\boldsymbol{n}_\perp}(\partial_{\boldsymbol{n}_\perp})$. The kernel $U_{2\mathrm{D}}$ is radially symmetric and given by

$$U_{2\mathrm{D}}(r)=\frac{\sqrt{\gamma_z}\mathrm{e}^{\gamma_z r^2/4}}{(2\pi)^{3/2}}K_0(\gamma_z r^2/4), \quad (8)$$

where K_ν (ν real) denotes a modified Bessel function of the second kind, and $r^2=(x-x')^2+(y-y')^2$.

For comparison, the corresponding 2D dimensionless GP equation for BECs in a rotating frame is provided

$$\mathrm{i}\frac{\partial\psi_{2\mathrm{D}}(x,y,t)}{\partial t} = \left\{\frac{1}{2}(\boldsymbol{P}-\boldsymbol{A})^2+\frac{1}{2}\left(1-\frac{\Omega^2}{\omega^2}\right)(x^2+y^2) +\beta\sqrt{\frac{\gamma_z}{2\pi}}\left[1-\varepsilon_{\mathrm{dd}}\left(1-3n_3^2\right)\right]|\psi_{2\mathrm{D}}|^2+\Phi_{2\mathrm{D}}\right\}\psi_{2\mathrm{D}}(x,y,t). \quad (9)$$

2.2. Numerical method

In the numerics, we use the norm-preserving imaginary time propagation method to solve Eqs. (6) and (9) on a 256 × 256 square grid.[24] The propagation continues until the fluctuation in the norm of the wave function becomes smaller than 10^{-6}. The spatial- and time-step sizes employed are 0.06 and 0.005, respectively. The two-dimensional Fourier transforms used in evaluating the dipolar potentials are implemented efficiently with a fast Fourier transform (FFT).

3. Results and discussion

To analyze the influence of DDI on the formation of a vortex, we numerically solve the time-dependent GP equation. Our main purpose is to investigate phenomena characteristic of the vortex formation in a dipolar BEC induced by a synthetic magnetic field. In what follows we discuss this issue by regulating the strength of the dipolar interaction, the rotating frequency, the aspect ratio of the trap, and the orientation of the dipole moment of the atoms with respect to their plane of motion. We would like to highlight the difference between the two models. Throughout this paper, we will use Ω_{c1}/ω and Ω_c/ω to denote the frequencies to generate a single vortex and certain number vortices, respectively.

3.1. The formation of vortices with respect to the dipole strength and the dipole orientation

We first study the formation of vortices in the system as a function of the orientation of the dipoles of the atoms with respect to their plane of motion and of the dipole strength. In Figs. 1 and 2, we show the two-dimensional atom densities for $\theta = 0°, 30°, 60°, 90°$ and several values of ε_{dd} in rotating frame and synthetic magnetic field, respectively. For comparison, we also plot the dependence of the critical rotating frequency Ω_{c1}/ω on ε_{dd} and θ in Fig. 3.

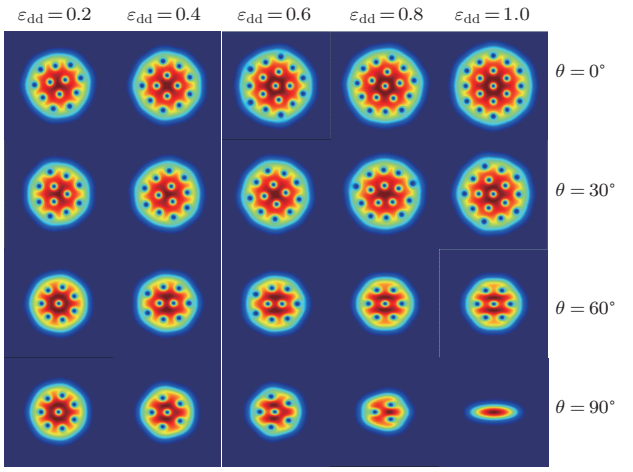


Fig. 1. (color online) Density profiles for the dipole strength ε_{dd} and the orientation of dipoles θ at $\beta = 100$ under rotating frequency $\Omega = 0.70\omega$ and aspect ratio $\gamma_z = 50$. From left to right, $\varepsilon_{dd} = 0.2, 0.4, 0.6, 0.8, 1.0$. From top to bottom, $\theta = 0°, 30°, 60°, 90°$. The field of view in the panels is $8a_0 \times 8a_0$. The color corresponds to the number of atoms, with red being the most and blue being the fewest.

From Figs. 1 and 2, we can see that the number of vortices changing as a function of ε_{dd} depends sensitively on the orientation of the dipoles. For example, when the polarization is along the z axis ($\theta = 0°$), the purely repulsive and isotropic nature of the dipolar interaction increases quickly the number of vortices as ε_{dd} increases. The number of vortices increases from 12 at $\varepsilon_{dd} = 0.2$ to 19 at $\varepsilon_{dd} = 1.0$ in the rotating frame case, while in the case of a synthetic magnetic field, the corresponding values are 7 and 13, respectively. As a consequence, Ω_{c1}/ω decreases with increasing ε_{dd}, as shown in Fig. 3.

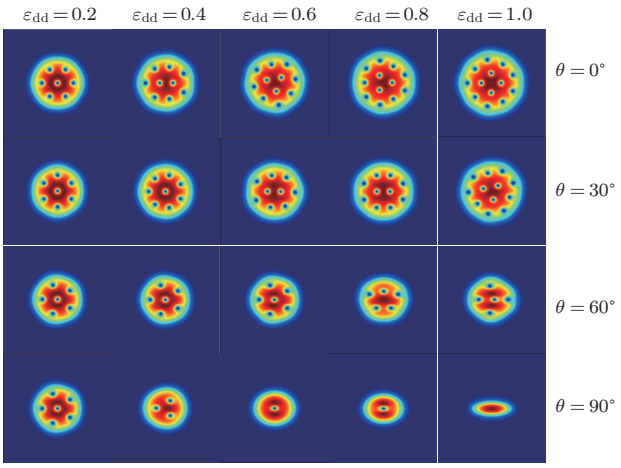


Fig. 2. (color online) Density profiles in a synthetic magnetic field.

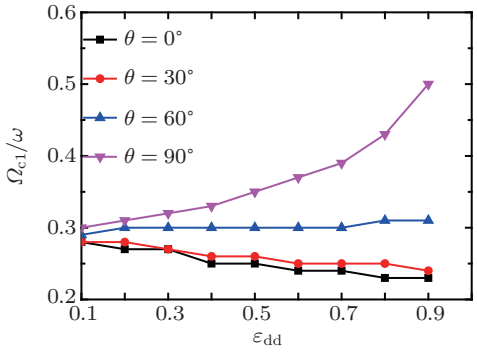


Fig. 3. (color online) The critical rotating frequency Ω_{c1}/ω as a function of the dipole strength ε_{dd} and the orientation of dipoles θ in a synthetic magnetic field. The parameters are fixed as $\gamma_z = 50$ and $\beta = 100$.

When the polarization angle becomes $\theta = 30°$, we find a similar behavior, the number of vortices increases and Ω_{c1}/ω decreases with increasing ε_{dd}, as in this case, the repulsive part of the dipole interaction still dominates the condensate.

For $\theta = 60°$, however, the dipolar interaction is mostly attractive. As a result, the number of vortices decreases and Ω_{c1}/ω increases with the increase of ε_{dd} in the considered range. It is different from that observed in Ref. [25], where the vortex number is independence of ε_{dd}.

When the angle becomes $\theta = 90°$, the behavior of the system changes. In this case, the attractive part of the dipole in-

teraction becomes dominant, preventing the formation of vortices. Thus the number of vortices decreases and Ω_{c1}/ω increases with increasing ε_{dd}. We also observe that the vortex number in the synthetic magnetic field is less than that in the rotating frame for the same dipole strength.

3.2. The formation of vortices with respect to the rotating frequency and the dipole orientation

We also study the formation of vortices as a function of the rotating frequency Ω and the dipole orientation θ for fixed $\beta = 100$ and $\varepsilon_{dd} = 0.8$. Figures 4 and 5 show the condensate densities in rotating frame and synthetic magnetic field, respectively. In the case of $\theta = 0^\circ$, the critical rotating frequencies Ω_{c1}/ω are 0.25ω and 0.24ω in rotating frame and synthetic magnetic field, respectively. The difference is very small. With further increasing rotating frequency, the two methods show obvious differences.

For the BEC confined in the rotating trap, the vortex number increases rapidly with increasing Ω. When the dipoles are polarized in-plane along the z axis ($\theta = 0^\circ$), the expansion of the density reported in the previous subsection due to the purely repulsive nature of the dipolar interaction accelerates the formation of vortices, especially when Ω approaches the trapping frequency ω. For example, there are 37 vortices at $\Omega = 0.90\omega$ and the vortex number increases to 57 at $\Omega = 0.99\omega$, which is just the upper limit of the rotating frequency. In the meantime, the system undergoes a transition from triangular lattice to stripe pattern. The stripe vortex lattices in the present study are not observed in Ref. [11].

The same qualitative behavior is found when the polarization angle θ is increased. Indeed, for $\theta = 30^\circ$, the main difference from the previous case is that the number presents a slight reduction.

The triangular lattice is, however, no longer observed for $\theta = 60^\circ$, regardless of the value of the rotating frequency. In this case, the stripe pattern occurs at earlier $\Omega = 0.80\omega$.

When the dipoles are polarized along the horizontal direction, i.e., when $\theta = 90^\circ$, the dipolar interaction is repulsive along the y axis and attractive along the x axis, as a consequence, the number of vortices decreases compared to that with $\theta = 60^\circ$ for the same rotating frequency.

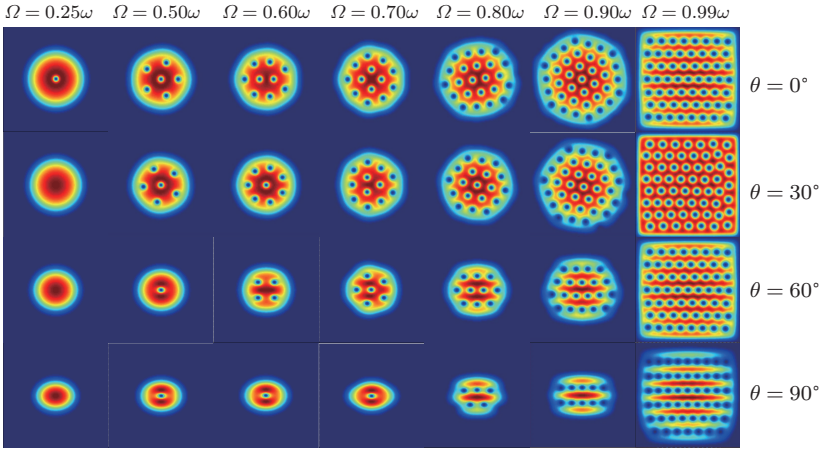


Fig. 4. (color online) Two-dimensional atom density distributions in the rotating frame. From left to right, $\Omega/\omega = 0.25$, 0.50, 0.60, 0.70, 0.80, 0.90, 0.99, and from top to bottom, $\theta = 0^\circ$, 30°, 60°, 90°. The trap aspect ratio is $\gamma_z = 30$, and the dipole strength is $\varepsilon_{dd} = 0.8$. The field of view in the panels is $8a_0 \times 8a_0$.

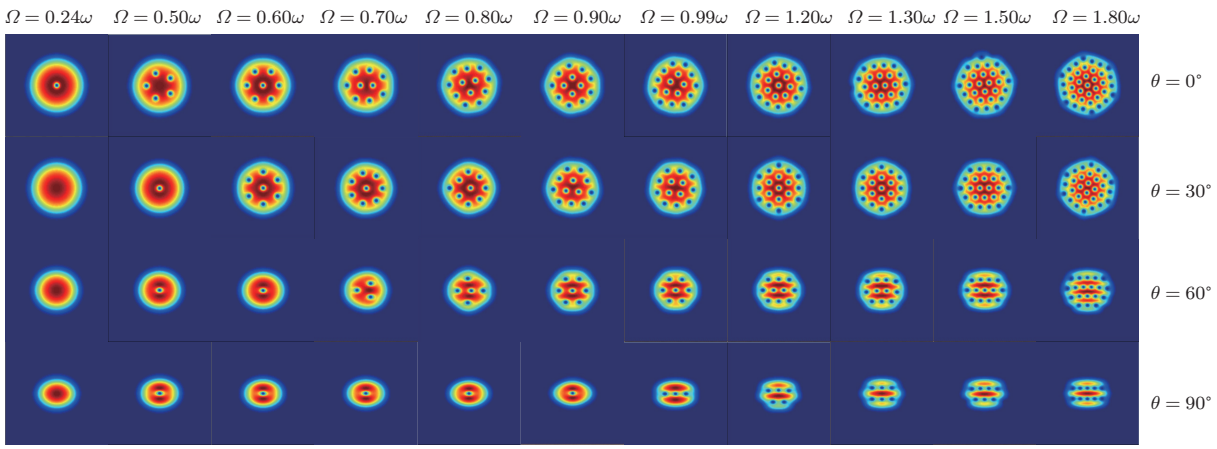


Fig. 5. (color online) Two-dimensional atom density distributions in the synthetic magnetic field. From left to right, $\Omega/\omega = 0.24$, 0.50, 0.70, 0.90, 0.99, 1.20, 1.30, 1.50, 1.80, and from top to bottom, $\theta = 0^\circ$, 30°, 60°, 90°. The trap aspect ratio is $\gamma_z = 30$, and the dipole strength is $\varepsilon_{dd} = 0.8$. The field of view in the panels is $8a_0 \times 8a_0$.

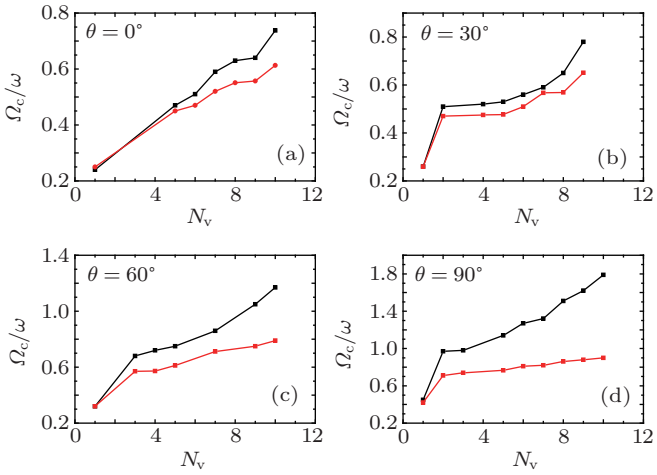


Fig. 6 (color online) Plots of the equilibrium vortex number N_v and the critical rotating frequency Ω_c/ω for conventional BECs with $\beta = 100$ and $\varepsilon_{dd} = 0.8$: (a) $\theta = 0°$, (b) $\theta = 30°$, (c) $\theta = 60°$, (d) $\theta = 90°$. The black and red lines represent the results of synthetic magnetic field and rotating frame, respectively.

In the synthetic magnetic field case, it is obvious that the vortex number grows much more slowly. Four cases are considered, namely, $\theta = 0°$, $30°$, $60°$, $90°$. In the case of $\Omega = 0.99\omega$, the corresponding numbers of vortices are 16, 13, 7, and 3, respectively. When the rotating frequency is increased to $\Omega = 1.80\omega$, the number of vortices increases, and the corresponding values become 37, 30, 19, and 10, respectively. In this large Ω case, no stripe pattern is obsevered for both $\theta = 0°$ and $30°$ cases and the vortex row number is reduced to 4 and 2 for the $\theta = 60°$ and $90°$ cases.

The above results show that it is hard for vortices to be created by the synthetic magnetic field. In order to elaborate this point further, we plot the dependence of the equilibrium vortex number N_v on critical rotating frequency Ω_c/ω in Fig. 6. In each case, we can see clearly that the critical rotating frequency in the synthetic field is larger than that in the rotating frame. Furthermore, we also observe that the anisotropy of dipolar interaction provides a directional preference to the condensate. For example, Ω_c/ω is 0.74 and 0.61 for $\theta = 0°$ in the synthetic field and the rotating frame, respectively. While in the case of $\theta = 90°$, the corresponding values are increased to 1.79 and 0.90. The latter is larger as compared to that of the former.

The explanation of these differences lies in the confinement of the trapping potential, Eq. (6) and (9). In the rotating frame, the effective trapping potential is reduced by the rotating frequency Ω, thus the atoms are pushed to peripheral sites of the potential easily. However, the trapping potential is not changed by the rotating frequency in the synthetic magnetic field.

As a natural extension, we also examine the Feynman rule in the synthetic magnetic field, which has been studied in the rotating frame.[26,27] The Feynman rule gives a relation that links the total number of vortices N_v with the rotating frequency Ω. For a superfluid rotating in a rigid container with radius R, by assuming a spatially homogeneous density, the number of vortices can be determined as[28]

$$N_v = \pi R^2 n_v = \frac{m\Omega R^2}{\hbar}, \tag{10}$$

where $n_v = m\Omega/\pi\hbar$ represents a uniform areal density, with a dense array of vortices. Alternatively, the Feynman rule can be expressed as $\langle L_z/\hbar\rangle = N_v/2$ with $\langle L_z/\hbar\rangle$ being the average of the angular momentum per atom averaged over the whole condensate.[27] This is because the mean angular momentum per atom is $\ell_z/\hbar = m\Omega r^2$ at position r. Then $\langle L_z/\hbar\rangle = \iint \psi^*(\ell_z/\hbar)\psi \mathrm{d}x\mathrm{d}y / \iint |\psi|^2 \mathrm{d}x\mathrm{d}y = m\Omega R^2/2\hbar$. Hence, one obtains $\langle L_z/\hbar\rangle = N_v/2$.

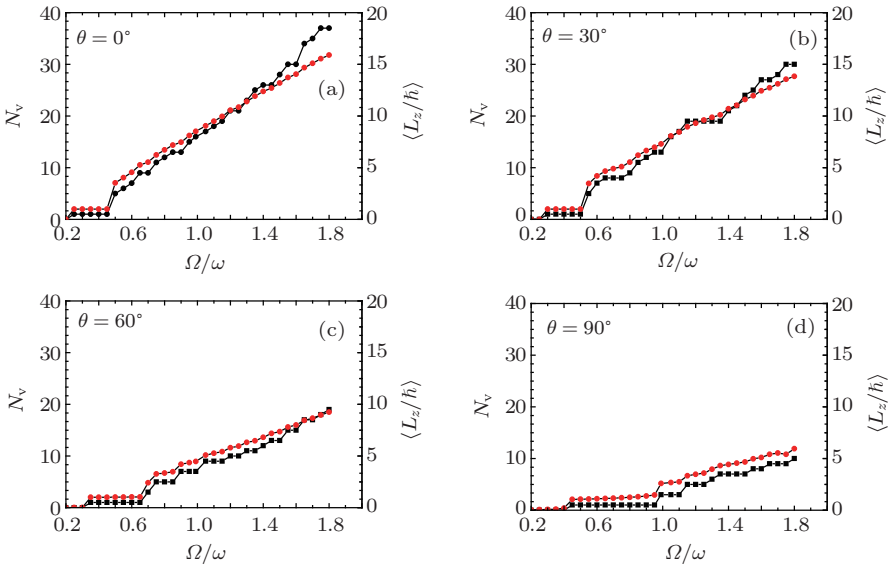


Fig. 7. (color online) The number of vortices N_v (black square points) and angular momentum per atom $\langle L_z/\hbar\rangle$ (red circle points) versus rotating frequency Ω/ω for conventional BECs in synthetic magnetic field with $\beta = 100$ and $\varepsilon_{dd} = 0.8$: (a) $\theta = 0°$, (b) $\theta = 30°$, (c) $\theta = 60°$, (d) $\theta = 90°$.

Figure 7 depicts the dependence of N_v and $\langle L_z/\hbar\rangle$ on Ω/ω for different θ in the synthetic magnetic field. The left coordinate values of N_v are two times the right coordinate values of $\langle L_z/\hbar\rangle$. The N_v is indicated by black square points and $\langle L_z/\hbar\rangle$ is symbolized by red circle points. The two lines are very close to each other. The results give good agreement with the Feynman rule. For the small deviations, one recalls the derivation, where the spatial density is assumed to be homogeneous. However, this cannot be guaranteed strictly during numerical calculation.

The most important results obtained in this section are summarized as follows. (i) The synthetic magnetic field can make the system remain stable at higher rotating frequency ($\Omega > \omega$). (ii) The number of vortices and the vortex row number are smaller in the synthetic magnetic field than those in the rotating frame at the same Ω. (iii) The synthetic magnetic is low efficient. In the next section, the effect of the aspect ratio will be discussed.

3.3. The formation of vortices with respect to the aspect ratio and the dipole orientation

In this section, we briefly discuss the effect of the trap aspect ratio, $\gamma_z = \omega_z/\omega$, on the formation of vortices. This issue has been discussed for 3-dimensional (3D) condensates in the rotating frame and it is indicated that increasing γ_z helps nucleation of the vortex.[29] Although the 3D system is converted into an effective 2D model in the present study, the trap aspect ratio γ_z can be quantitatively considered since it is included in equivalent contact interaction $\beta\sqrt{\gamma_z/2\pi}[1-\varepsilon_{dd}(1-3n_3^2)]$. As shown in Fig. 8, the critical rotating frequency for the single-vortex state, Ω_{c1}/ω, decreases with increasing trap aspect ratio, consistent with the results for the 3D BEC.

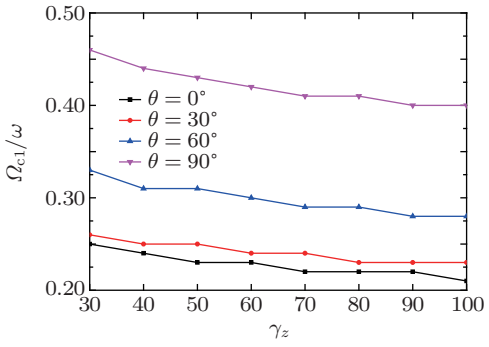


Fig. 8. (color online) The critical rotating frequency Ω_{c1}/ω as a function of the aspect ratio γ_z and the orientation of dipoles θ in synthetic magnetic field. The constants are taken as $\varepsilon_{dd} = 0.8$ and $\beta = 100$.

In Figs. 9(a) and 9(b), we depict the atom density as a function of γ_z in a rotating frame for $\theta = 0°$ and $\theta = 90°$, respectively. The corresponding results for a synthetic magnetic field are given in Figs. 9(c) and 9(d). One may note that, in Figs. 9(a)–9(c), the vortex number increases with increasing trap aspect ratio. Increasing γ_z means that the atoms are forced to assemble on the xy plane, then the condensate size on the xy plane expands. This allows the formation of more vortices in the condensate. Whereas, in Fig. 9(d), we observe that even though γ_z reaches the higher value 100, the vortex number remains unchanged. The reason may be the stronger confinement of the trap and mostly attractive of the dipolar interaction. We also observe that the vortex number in the synthetic magnetic field is smaller than that in the rotating frame for the same aspect ratio.

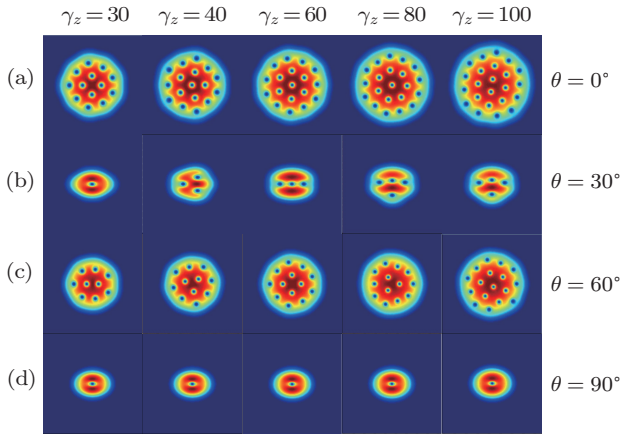


Fig. 9. (color online) Profiles of density $|\psi_{2D}|^2$ for (a), (b) rotating frame and (c), (d) synthetic magnetic field. The constants are taken as $\beta = 100$ and $\Omega = 0.80\omega$. The field of view in the panels is $8a_0 \times 8a_0$.

4. Conclusion

We investigate the formation of vortices in a dipolar BEC in a synthetic magnetic field. In contrast to the rotating frame case where the system is unstable when the rotating frequency Ω is larger than the radial trap oscillator frequency ω, the strong confinement in the synthetic magnetic field can lead the system to remain stable at higher rotating frequency ($\Omega > \omega$). We find that the number of vortices generated by the synthetic magnetic field is much smaller than that by the rotating frame under the same condition, which reveals that the synthetic magnetic field is less efficient in creating vortices. We also confirm that strengthening the dipole strength or increasing the trap aspect ratio can create more vortices. Finally, the validity of the Feynman rule is checked.

Acknowledgment

QZ thanks Weizhu Bao for technical assistance in the numerical simulations and Junjun Xu for reading the manuscript carefully.

References

[1] Griesmaier A, Werner J, Hensler S, Stuhler J and Pfau T 2005 *Phys. Rev. Lett.* **94** 160401
[2] Lu M, Burdick N Q, Youn S H and Lev B L 2011 *Phys. Rev. Lett.* **107** 190401
[3] Aikawa K, Frisch A, Mark M, Baier S, Rietzler A, Grimm R and Ferlaino F 2012 *Phys. Rev. Lett.* **108** 210401

[4] Lahaye T, Menotti C, Santos L, Lewenstein M and Pfau T 2009 *Rep. Prog. Phys.* **72** 126401
[5] Baranov M A, Dalmonte M, Pupillo G and Zoller P 2012 *Chem. Rev.* **112** 5012
[6] Vengalattore M, Leslie S R, Guzman J and Stamper-Kurn D M 2008 *Phys. Rev. Lett.* **100** 170403
[7] Eto Y, Saito H and Hirano T 2014 *Phys. Rev. Lett.* **112** 185301
[8] Bismut G, Pasquiou B, Maréchal E, Pedri P, Vernac L, Gorceix O and Laburthe-Tolra B 2010 *Phys. Rev. Lett.* **105** 040404
[9] Lahaye T, Koch T, Fröhlich B, Fattori M, Metz J, Griesmaier A, Giovanazzi S and Pfau T 2007 *Nature* **448** 672
[10] Cooper N R, Rezayi E H and Simon S H 2005 *Phys. Rev. Lett.* **95** 200402
[11] Yi S and Pu H 2006 *Phys. Rev. A* **73** 061602(R)
[12] Zhang J and Zhai H 2006 *Physics* **35** 0 (in Chinese)
[13] Liu C F, Wan W J and Zhang G Y 2013 *Acta Phys. Sin.* **62** 200306 (in Chinese)
[14] Wang X, Tan R B, Du Z J, Zhao W Y, Zhang X F and Zhang S G 2014 *Chin. Phys. B* **23** 070308
[15] Chen G P 2015 *Acta Phys. Sin.* **64** 030302 (in Chinese)
[16] Lahaye T, Metz J, Fröhlich B, Koch T, Meister M, Griesmaier A, Pfau T, Saito H, Kawaguchi Y and Ueda M 2008 *Phys. Rev. Lett.* **101** 080401
[17] Dum R, Cirac J I, Lewenstein M and Zoller P 1998 *Phys. Rev. Lett.* **80** 2972
[18] Williams J E and Holland M J 1999 *Nature* **401** 568
[19] Stringari S 1999 *Phys. Rev. Lett.* **82** 4371
[20] Lin Y L, Compton R L, Perry A R, Phillips W D, Porto J V and Spielman I B 2009 *Phys. Rev. Lett.* **102** 130401
[21] Lin Y L, Compton R L, Jiménez-García K, Porto J V and Spielman I B 2009 *Nature* **462** 628
[22] Zhao Q and Gu Q 2015 *Front. Phys.* **10** 100306
[23] Cai Y Y, Rosenkranz M, Lei Z and Bao W Z 2010 *Phys. Rev. A* **82** 043623
[24] Bao W Z, Wang H Q and Markowich P A 2005 *Commun. Math. Sci.* **3** 57
[25] Malet F, Kristensen T, Reimann S M and Kavoulakis G M 2011 *Phys. Rev. A* **83** 033628
[26] Kasamatsu K, Tsubota M and Ueda M 2003 *Phys. Rev. A* **67** 033610
[27] Wen L H, Xiong H W and Wu B 2010 *Phys. Rev. A* **82** 053627
[28] Feynman P R 1955 *Prog. Low Temp. Phys.* **1** 17
[29] Santos L, Shlyapnikov G V, Zoller P and Lewenstein M 2000 *Phys. Rev. Lett.* **85** 1791